



# Electronic correlation and transport properties of nuclear fuel materials

Quan Yin,\* Andrey Kutepov, Kristjan Haule, and Gabriel Kotliar

*Department of Physics and Astronomy, Rutgers University, Piscataway, New Jersey 08854, USA*

Sergey Y. Savrasov and Warren E. Pickett

*Department of Physics, University of California, Davis, California 95616, USA*

(Received 26 September 2011; published 8 November 2011)

The electronic structures and transport properties of a series of actinide monocarbides, mononitrides, and dioxides are studied systematically using a combination of density-functional theory and dynamical mean-field theory. The studied materials present different electronic correlation strength and degree of localization of  $5f$  electrons, where a metal-insulator boundary naturally lies within. In the spectral function of Mott-insulating uranium oxide, a resonance peak is observed in both theory and experiment and may be understood as a generalized Zhang-Rice state. We also investigate the interplay between electron-electron and electron-phonon interactions, both of which are responsible for the transport in the metallic compounds. Our findings allow us to gain insight in the roles played by different scattering mechanisms, and suggest how to improve their thermal conductivities.

DOI: [10.1103/PhysRevB.84.195111](https://doi.org/10.1103/PhysRevB.84.195111)

PACS number(s): 71.27.+a, 28.41.Bm

## I. INTRODUCTION

When engineering fuel materials for nuclear power, important thermophysical properties to be considered are melting point and thermal conductivity. Understanding the physics underlying transport phenomena due to electrons and lattice vibrations in actinide systems is a crucial step toward the design of better fuels. In this work we conduct a systematic theoretical study on the electronic structures and lattice dynamics of actinide compounds. We start by concentrating on the class of actinide oxides, nitrides, and carbides based on uranium, neptunium, plutonium, americium, and curium. According to the Lindemann criterion, solids with large Debye frequencies have high melting points. This is typically found in insulators where atomic bonds are strong due to lack of electronic screening. On the other hand, high thermal conductivity can usually be achieved in metals where conduction electrons are dominant heat carriers. For example, uranium and plutonium oxide fuels used in very high-temperature fast breeder reactors have very high melting points, but they suffer from poor thermal conductivity. Hence attention is turning to metallic fuels for the new generation of reactors, such as uranium carbide and nitride.<sup>1</sup> Applying these principles to the actinide compounds leads us to an observation that systems close to the Mott transition from the metallic side are the best option. In the present work we thoroughly study the transport properties of uranium monocarbide and mononitride, two promising metallic fuel materials, and prescribe how to improve them by intercalating solid solution.

## II. COMPUTATIONAL METHODS

### A. LDA+DMFT

Electronic structures and thermophysical properties of actinide compounds are not well described by the traditional approaches based on density-functional theory (DFT) within its local-density approximation (LDA) due to strong electronic correlation. It requires a theory that can take into account both itinerant and localized behaviors of the correlated electrons

on equal footing. In this study we use an advanced electronic structure method based on the combination of DFT and dynamical mean-field theory (LDA+DMFT),<sup>2</sup> which has proven success in describing such strongly correlated problems.<sup>3-5</sup> Our full-potential charge self-consistent implementation of LDA+DMFT described in Ref. 6 is based on the DFT program WIEN2K.<sup>7</sup> For the impurity solver we use the continuous time quantum Monte Carlo (CTQMC) algorithm.<sup>8,9</sup> For late actinides such as Pu and beyond, we use the less expensive vertex corrected one-crossing approximation (OCA),<sup>2</sup> which is very accurate in these more localized systems. All calculations were performed in the paramagnetic phase, using experimental structural parameters and scalar relativistic including spin-orbit coupling.

### B. Linear-response method of lattice dynamics

For the calculation of phonon spectra we used the well developed full-potential density-functional linear-response approach implemented in the linear muffin-tin orbital (LMTO) basis,<sup>10,11</sup> which has successfully produced the lattice dynamics of many solids<sup>12</sup> including actinides materials such as plutonium<sup>3</sup> and UO<sub>2</sub>.<sup>5</sup> The spin-orbit coupling effect is included in this calculation. A  $\mathbf{q}$  grid of  $6 \times 6 \times 6$  is used to compute phonon frequencies, which generates 36 irreducible  $q$  points in the Brillouin zone.

## III. CORRELATION STRENGTH AND ELECTRONIC STRUCTURES

We first describe the chemical trends governing the degree of localization of the  $f$  electrons in the binary actinide compounds listed in Fig. 1. The key parameters are the on-site Coulomb repulsion among the  $5f$  electrons, quantified by the Hubbard  $U$  and Hund's rule exchange  $J$ ; the charge-transfer energy  $\Delta$ ; and the  $5f$  bandwidth quantified by the hybridization between  $5f$  and  $spd$  electrons.

While most electronic structure methods can accurately calculate the hopping integrals between various electronic



FIG. 1. (Color online) Correlation diagram. The shading represents the electronic correlation strength. The labels on the top denote the actinide elements, and the labels to the left denote the ligand elements. The red line is the metal-insulator boundary. Two quantities, which are computed at  $T = 100$  K, are listed in each cell: Hubbard  $U$  (units: eV) and  $f$ -electron valence  $n_f$ .

orbitals, evaluating the screened  $U$  in solids is generally a difficult task. Here we have computed  $U$  using a newly developed fully self-consistent many-body GW approach,<sup>13</sup> which provides a seamless interface with LDA+DMFT. The latter method allows us to determine the degree of localization of the  $5f$  electrons in each material. Our estimates for the Hund’s  $J$  are within the range 0.5–0.6 eV, about 30% smaller than their atomic values due electronic screening. This set of Coulomb interaction  $U$  parameters are somewhat larger than what have been used in previous theoretical studies because LDA+DMFT, when solved by an exact impurity solver, sums up all local diagrams, many of which screen Coulomb interaction efficiently, and thus requires a larger  $U$ .

The charge-transfer energy  $\Delta$  is computed as the energy difference between the center of  $p$  band of ligand (C, N, or O) atoms and  $5f$  band of actinides, and listed in Table I.  $\Delta$  increases from carbides to oxides due to the stronger electronegativity of the ligand atoms.  $\Delta$  decreases from U to Cm compounds because as the atomic number  $Z$  increases, the  $5f$  occupation grows and the  $5f$  band is pulled lower with respect to the ligand  $p$  band. The charge-transfer energy increases vertically from carbides to oxides due to the change in the electronegativity of ligand atoms. The bandwidth of  $5f$  electrons shrinks horizontally from U to Cm compounds, indicating a more localized nature in late actinides. This causes a reduction of screening, which is manifest in the gradual increase of  $U$  from the left to the right, and from the top to the bottom of the table. The charge-transfer energies of oxides, from UO<sub>2</sub> to CmO<sub>2</sub>, range from 3.8 to 2.5 eV, smaller than their Coulomb  $U$  values.

As a combination of the above quantities, the overall correlation strength and localization is visualized by the shading of Fig. 1, referred to as the “correlation diagram” of binary nuclear fuel materials, where the gray gradient

TABLE I. The calculated charge-transfer energy of the 15 studied compounds. The units are eV.

	U	Np	Pu	Am	Cm
C	2.27	1.96	1.78	0.92	0.67
N	3.14	2.55	2.07	1.64	1.39
O <sub>2</sub>	3.79	3.53	3.41	2.75	2.49

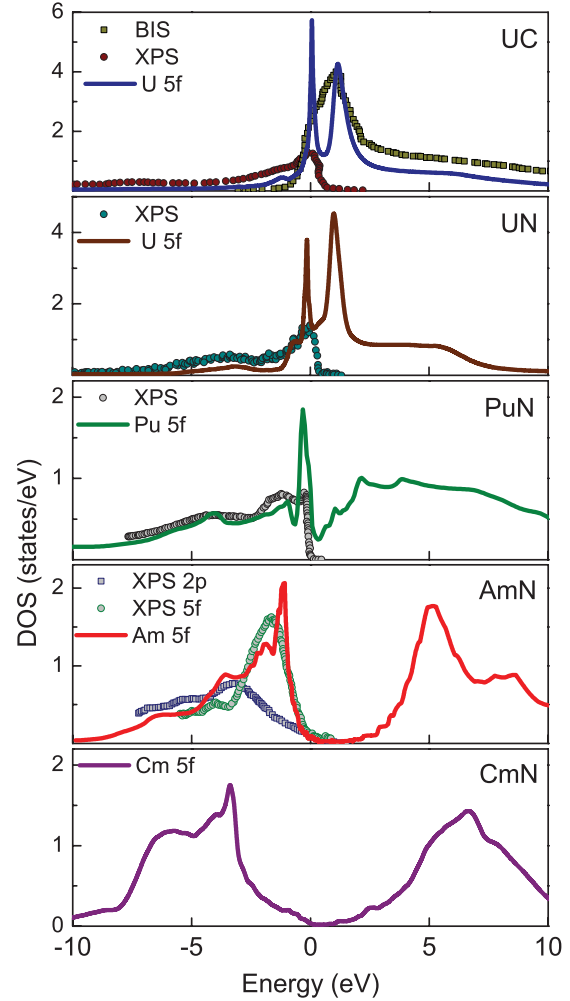


FIG. 2. (Color online) Partial  $5f$  DOS of UC, UN, and select actinide nitrides, calculated at  $T = 100$  K, and compared with available x-ray photoemission spectroscopy. The XPS and BIS data of UC are from Ref. 14, UN from Ref. 15, PuN from Ref. 16, and AmN from Ref. 17.

approximately represents the partial  $f$  density of states at the Fermi level computed by LDA+DMFT.

Next, we present the frequency dependence of the electronic spectral functions of some representative compounds in Fig. 2. From the top panel to the bottom, the  $5f$  partial density of states (DOS) changes qualitatively. UC and UN represent an itinerant  $5f$ -electron system with most spectral weight on the Fermi level, but the picture starts to change at PuN, where the Kondo resonance and satellite  $5f$  states are present. In AmN the  $5f$  DOS begins to form an marginal energy gap. The evolution of the density of states from UN to CmN echoes the itinerancy-localization transition of  $5f$  electrons, and demonstrates the metal-insulator transition in a transparent point of view. CmC, CmN, and all the actinide oxides are also found to be insulators. This allows us to establish a metal-insulator transition boundary, illustrated by the thick red line in Fig. 1.

The actinides ions in most of the metallic crystals are found to be in a mixed-valence state, where they do not settle in one valence, but fluctuate between different valences in the

solid. It can be described by an effective number  $n_f$  (listed in Fig. 1), obtained using a valence histogram technique,<sup>4</sup> which represents an average over all the atomic configurations weighted by corresponding probabilities.

As for the two metallic uranium compounds, which we will focus on in transport properties, experimentally UC is a Fermi liquid (FL) at room temperature and angle-resolved photoemission spectroscopy (ARPES) measurement indicates that the overall bandwidth is reduced by a factor of 4 relative to the LDA band structure.<sup>18</sup> In our calculation UC is a FL below 300 K with  $m^*/m_{\text{LDA}} = 3.7$ . On the other hand, UN shows a strongly correlated heavy fermion character with a coherence temperature below its Néel temperature of 53 K. In the absence of magnetic order, UN would be a FL at very low temperature with a large mass enhancement ( $m^*/m_{\text{LDA}} \approx 12$ ) as can be inferred from the linear specific-heat coefficient.<sup>19</sup> It is a non-FL in the temperature range (55–1000 K) we studied.

We now turn to the electronic structure of oxides. Hybrid functionals, especially the newly developed Heyd-Scuseria-Ernzerhof (HSE) variant, which mixes a certain amount of Hartree-Fock exact exchange potential with LDA/generalized gradient approximation (GGA) potentials, has successfully captured strong correlation effects and produced qualitatively correct spectral properties, energy gaps, and accurate optimal lattice constants in actinide oxides.<sup>20,21</sup> However, in these studies the spin-orbit coupling was not considered and the calculations were done in either the ferromagnetic (FM) or antiferromagnetic (AFM) state. As a generalization to DFT by adding static Hartree-Fock mean-field approximation of electron interactions, the LDA+U is widely used for electronic structure calculation of strongly correlated materials, and has been applied on actinide oxides such as  $\text{UO}_2$ ,<sup>22</sup>  $\text{NpO}_2$ ,<sup>23</sup> and  $\text{PuO}_2$ .<sup>24</sup> Although some calculated physical properties were improved over LDA, the LDA+U relies on magnetic ordering to get the correct energy gap, and it does not capture real atomic features nor quasiparticle bands, and thus fails in correlated metallic compounds. LDA+DMFT does not require the magnetic ordering to obtain the Mott insulating gap. The total and partial DOS of  $\text{UO}_2$  and  $\text{PuO}_2$  calculated by LDA+DMFT are shown in Fig. 3. Both are Mott insulators with well formed Hubbard bands and large correlation energy gaps. Most noticeably, the situation  $U > \Delta$  allows us to describe the insulating actinide oxides as charge-transfer Mott insulators,<sup>27</sup> which is well known from late transition-metal oxides, for example NiO, the classical textbook example of strongly correlated systems.<sup>28</sup>

As it is known from cuprates, which are charge-transfer-type Mott insulators, that the Zhang-Rice state (ZRSs)<sup>29</sup> would appear as the low-energy resonance corresponding to the coupling of local moments of correlated electron orbitals to the hole induced by phototemission process on ligand orbitals. This ZRS concept has been generalized to other transition-metal oxides,<sup>28</sup> since they have the same physics as cuprates. In the case of  $\text{UO}_2$ , the situation is very similar because it also has a charge-transfer energy gap, and there is a local magnetic moment on the U  $5f^2$  orbital due to the  $\Gamma_5$  triplet being its many-body ground state. On the other hand,  $\text{PuO}_2$  does not have the ZRS because its ground state of the  $5f^4$  shell is the  $\Gamma_1$  singlet, which as zero moment. Since Hubbard bands are of atomic nature, the position of

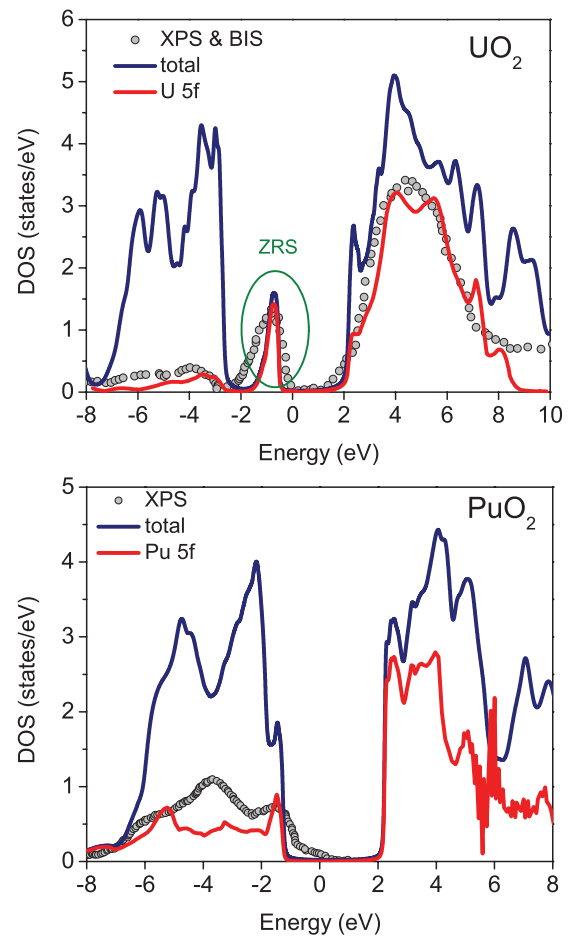


FIG. 3. (Color online) (a) Total and partial DOS of  $\text{UO}_2$ . XPS and BIS taken from Ref. 25. (b) Total and partial DOS of  $\text{PuO}_2$ . XPS from Ref. 26. Both calculated at  $T = 100$  K.

the lower Hubbard band (LHB) is found numerically by computing the many-body excitation energy of the impurity problem of DMFT, i.e.,  $E(f^2) - E(f^1)$ . In the theoretical spectral function of  $\text{UO}_2$ , the LHB is located at about  $-4.3$  eV, which is broad and hybridized heavily with the O  $2p$  band. By performing the same calculation with other values of  $U$ , we

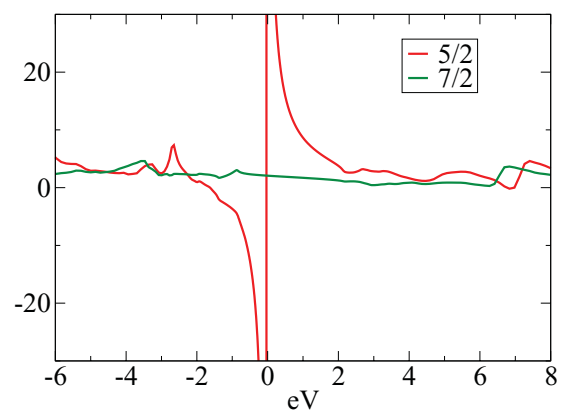


FIG. 4. (Color online) The real part of self-energy of  $\text{UO}_2$  on real frequency axis.

found that this resonance peak is not sensitive to the choice of  $U$ , while the Hubbard bands shift proportionally to  $U$ . Since DMFT corrects LDA spectral function via the self-energy, the formation of ZRS can also be explained through the self-energy of UO<sub>2</sub>, plotted in Fig. 4. The strong divergent peak in the relevant 5/2 orbital at the Fermi energy (EF) is what splits the  $f$  band of LDA and creates the two Hubbard bands. The other small peak in 5/2 channel, at about  $-2.5$  eV, is responsible for the resonance  $f$  peak (ZRS) in the DOS just below EF.

#### IV. TRANSPORT PROPERTIES

##### A. Electronic correlation and transport

After understanding the electronic structures, we turn to the transport properties. We focus on correlated metallic compounds, where electrons play the role of charge and heat transporters, while retaining a high melting point. Although in normal metals electron-phonon scattering is dominant except at very low temperatures, in strongly correlated metals electron-electron scattering takes the lead. The electronic contribution to thermal conductivity is proportional to the electrical conductivity via the Wiedemann-Franz law. From the electronic structure and correlation strength of the studied materials, small resistivity occurs in the least correlated compounds in our table. Indeed UC and UN are the best fuel materials in terms of their outstanding transport properties.

Strong Coulomb interactions among electrons can substantially reduce the interaction between electrons and lattice vibrations.<sup>30</sup> Hence the electron-phonon interaction (EPI) is usually weaker in strongly correlated materials, which might lead to smaller resistivity due to EPI. On the other hand, increasing electronic correlations leads to an increase in resistivity due to electron-electron scattering. Therefore neither extremely weak nor strong correlations are good from the perspective of minimizing resistivity. Deciding the optimal degree of correlation for the purpose of maximizing conductivity thus requires first-principle calculations.

To evaluate the conductivity due to electron-electron scattering we use the Kubo formalism,<sup>6</sup> where the scattering rate comes from the imaginary part of DMFT self-energy  $\Sigma(\omega, T)$ , obtained from CTQMC.

##### B. Phonons and electron-phonon interactions

The phonon dispersion of UN along three high-symmetry directions is plotted in Fig. 5(a) together with experimental data measured by neutron scattering.<sup>31</sup> As shown in Fig. 5(b), UC carries similar phonon dispersions but slightly lower phonon energies. Despite the apparent presence of correlation effects, excellent agreement is achieved with the local-density approximation (LDA). Similar success of LDA in studying lattice dynamics of strongly correlated metallic systems have been reported earlier, for example, in palladium,<sup>12</sup> high-temperature superconducting cuprates,<sup>32</sup> and recently iron pnictides.<sup>33</sup>

Calculations of electron-phonon interactions and transport properties require quasiparticle description of the one-electron spectra when evaluating Eliashberg and transport spectral

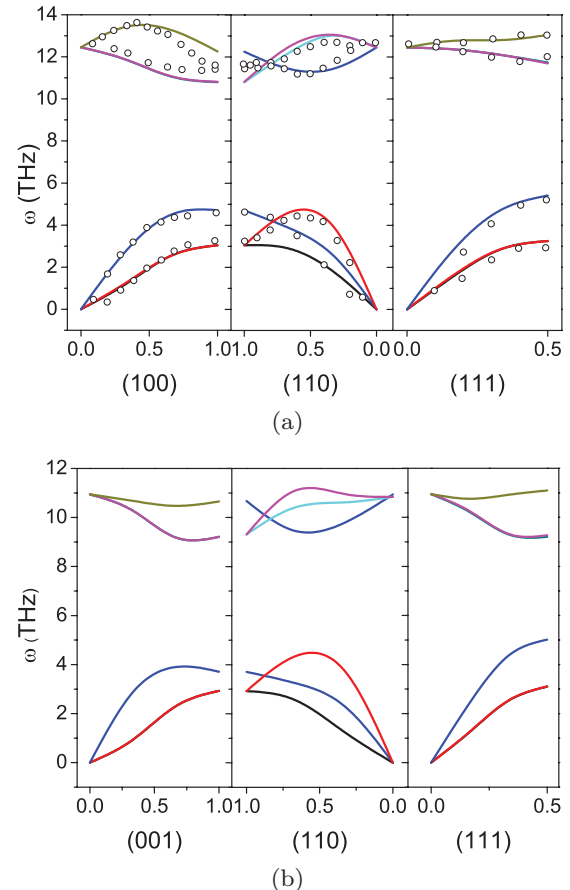


FIG. 5. (Color online) Phonon dispersions plotted along three high-symmetry lines. (a) Solid curves: Calculated phonon dispersion of UN. Open circles: Experimental phonon excitations of UN from Ref. 31. (b) Theoretical phonon dispersion of UC.

functions by integrating over the Fermi surfaces.<sup>12</sup> As a result, due to large mass enhancement, the straightforward LDA procedure can produce wrong electron-phonon resistivity, which was indeed found in our calculation for UC where  $\rho(T)_{\text{EPI}}$  was overestimated by a factor of 3 compared to experiment. This is despite of simple arguments that would suggest that any multiplicative effects on the electron mass renormalization should cancel out in the resistivity, because it enters both the scattering rate  $\tau$  that appears in the denominator, and the electronic mass that appears in the numerator of the expression for  $\rho(T)_{\text{EPI}}$ , which is evident from a simple Drude formula for  $\rho = m/(ne^2\tau)$ . However, in general, this does not apply to multiband systems where only correlated  $f$ -electron wave functions are primarily affected by strong Coulomb interactions.

In order to evaluate the electron-phonon scattering in the presence of correlations we develop a method that accounts for the effects from quasiparticle mass renormalization and spectral weight transfer by utilizing interacting Green functions. We have previously shown<sup>34</sup> that the use of the pole interpolation of self-energy,

$$\Sigma(\omega) = \Sigma(\infty) + \sum_i \frac{V_i^\dagger V_i}{\omega - P_i}, \quad (1)$$

allows us to replace the nonlinear (over energy) Dyson equation by a linear Schrodinger-like equation in an extended subset of “pole states”:

$$\begin{pmatrix} \omega - H_0(\mathbf{k}) - \Sigma(\infty) - \epsilon_{\mathbf{k}j} & V^+ \\ V & \omega - P - \epsilon_{\mathbf{k}j} \end{pmatrix} \begin{pmatrix} \psi_{\mathbf{k}j}^{(e)} \\ \psi_{\mathbf{k}j}^{(a)} \end{pmatrix} = 0. \quad (2)$$

Here, only components  $\psi_{\mathbf{k}j}^{(e)}$  describe one-electron excitations where the spectral content of each energy eigenvalue  $\epsilon_{\mathbf{k}j}$  is determined by the matrix element  $\langle \psi_{\mathbf{k}j}^{(e)} | \psi_{\mathbf{k}j}^{(e)} \rangle$  that is less than unity in general. The advantage of the present method is that the well developed machinery of standard electronic structure methods can be simply generalized to account for the dynamical self-energy effects. In particular, our successful applications on computation of phonon spectra in paramagnetic states of Mott insulators such as NiO,<sup>35</sup> UO<sub>2</sub>, and PuO<sub>2</sub>,<sup>5</sup> as well as in Pu,<sup>3</sup> and Am,<sup>34</sup> as representative systems with localized  $f$  electrons have been made with the Hubbard 1 self-energy that exactly casts the form of the pole expansion in Eq. (1).

In the present work we extend this method to compute electron-phonon interactions for systems such as UC and UN whose  $f$  electrons show itinerant behavior with  $m^*/m_{\text{LDA}} \approx 4$ –12. To capture this mass renormalization effect, we first make a fit to the self-energy obtained from the CTQMC, using a two-pole interpolation where the slope of the self-energy at zero frequency  $d\Sigma(\omega)/d\omega|_{\omega=0} = 1 - m^*/m_{\text{LDA}}$  controls the electronic mass enhancement while the positions of the two poles  $P_i$  in Eq. (1) determine the transfer of the spectral weight from the quasiparticle band to the Hubbard bands. Second, we assume that the  $f$  electrons are rigidly bound to their ions so that there is no actual change in the self-energy,  $\delta\Sigma(\omega)$ , caused by ionic excursions from their equilibrium positions. Since the main contribution to electronic transport comes from the states near the Fermi surface, where quasiparticles are best described in terms of slave bosons, the neglecting of  $\delta\Sigma(\omega)$  due to ion displacements corresponds to a rigid self-energy approximation. This is very similar to the famous rigid muffin-tin approximation (RMTA),<sup>36</sup> which has been successfully applied in the past to study electron-phonon interactions in transition-metal materials.<sup>37,38</sup> Therefore our use of rigid self-energy is expected to demonstrate a similar accuracy.

As a result, the electron-phonon scattering matrix element  $g_{\mathbf{k}j\mathbf{k}+\mathbf{q}j'}$  can be evaluated using the electronic components  $\psi_{\mathbf{k}j}^{(e)}$  that appear as solutions to Eq. (2), and the change of the ground-state LDA potential,  $\delta^q V_{\text{LDA}}$ , computed for each phonon wave vector  $\mathbf{q}$ , i.e.,

$$g_{\mathbf{k}j\mathbf{k}+\mathbf{q}j'} = \langle \psi_{\mathbf{k}j}^{(e)} | \delta^q V_{\text{LDA}} | \psi_{\mathbf{k}+\mathbf{q}j'}^{(e)} \rangle.$$

These matrix elements can be subsequently used for evaluating the EPI part of electrical and thermal resistivity similar to our previous applications on weakly correlated metals,<sup>12</sup> where the corresponding Fermi-surface integrals are now performed with “band structures”  $\epsilon_{\mathbf{k}j}$  of Eq. (2) that acquire renormalizations due to correlations. Finally, the EPI resistivity can be computed by

$$\rho_{\text{EPI}}(T) = \frac{\pi \Omega_{\text{cell}} k_B T}{N(E_F) \langle v_x^2 \rangle} \int \frac{x^2}{\sinh^2 x} \frac{\alpha^2 F(\omega)}{\omega} d\omega. \quad (3)$$

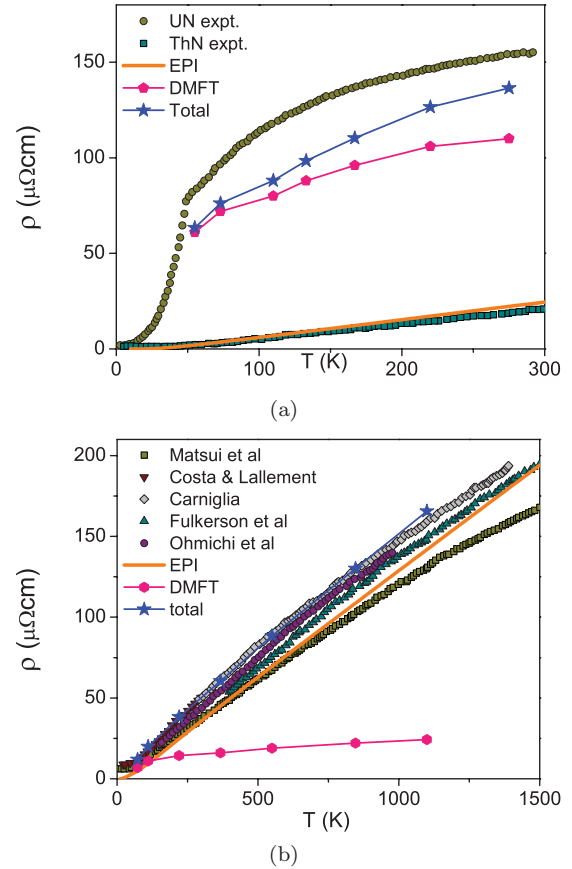


FIG. 6. (Color online) Electrical resistivity due to two different scattering mechanisms. The electron-phonon interaction (EPI) resistivity is shown as solid lines, and electron-electron interaction resistivity, which is calculated by LDA+DMFT (CTQMC) at several temperatures, is shown as solid hexagons connected by lines. The total resistivity  $\rho(T)_{\text{total}} = \rho(T)_{ee} + \rho(T)_{\text{EPI}}$  is shown as stars connected by lines. (a) UN. Experimental resistivity data are taken from Ref. 15. (b) UC. Experimental data after Refs. 39–43. The Debye and Kondo temperatures are UN:  $\Theta_D = 332$  K,  $T_K = 1720$ ; UC:  $\Theta_D = 320$  K,  $T_K = 5500$ .

Since the inclusion of correlation effects also renormalizes bands and thus modifies the Fermi surface as well as the average electron velocity, which enters the denominator of Eq. (3), the combined effect of electron correlation on  $\rho_{\text{EPI}}(T)$  is not straightforwardly seen. By applying this theory, we have obtained a substantial reduction (by a factor of 3) in  $\rho(T)_{\text{EPI}}$  for UC, while in UN the effect was marginal.

### C. Total transport properties

Taking into account both electron-electron and electron-phonon scattering mechanisms, we can now build the entire picture of the electronic transport in the uranium compounds with our results summarized in Fig. 6. Electron-electron scattering can account for approximately 80% of  $\rho(T)$  in UN, commonly found in heavy fermion systems, entitling it as a strongly correlated bad metal. In contrast, UC shows nearly linear  $\rho(T)$ , which is an indication of dominant electron-phonon scattering, and our calculated results indeed show that in UC,  $\rho(T)_{ee}$  is much smaller than  $\rho(T)_{\text{EPI}}$ . The  $\rho_{\text{EPI}}(T)$

of UN shows very similar behavior, both qualitatively and quantitatively, to the experimental resistivity of ThN, which has no  $5f$  electrons and thus its resistivity is purely due to electron-phonon interaction. This comparison reflects the strong electron-electron correlation in UN, which acts as additional (and in this case major) scattering of electrons. Our calculations verify the distinct characters in the electrical transport of UC and UN, two seemingly similar materials.

While electrical current can only be carried by electrons in solids, excitations other than electrons may contribute to thermal conductivity. Here we also estimate lattice vibrational contribution to thermal conductivity in UC and UN, using the phonon spectra we obtained from linear-response calculation. This is done by evaluating the Gruneisen parameter and phonon group velocities using the method described previously for MOX fuels.<sup>5</sup> According to our result, at  $T = 1000$  K, lattice thermal conductivity  $\kappa_{\text{ph}}$  is equal to 2.7 W/mK in UC, and  $\kappa_{\text{ph}} = 4.4$  W/mK in UN. Thus  $\kappa_{\text{ph}}$  only plays a minor role in these two metallic uranium compounds.

We put together our results and evaluate total thermal conductivity at 1000 K, a representative temperature under which nuclear reactors operate. By applying the Wiedemann-Franz law on the electrical conductivity data, we obtain  $\kappa_{ee}$ . Since electronic thermal resistivity consists of two scattering processes, total thermal conductivity is estimated by  $\kappa_{\text{total}} = (\kappa_{ee}^{-1} + \kappa_{\text{EPI}}^{-1})^{-1} + \kappa_{\text{ph}}$ , in which the first two terms correspond to  $\kappa_{\text{electron}}$ . For UN, our result,  $\kappa_{\text{total}} = 16.5$  W/mK, compares well with a recent study which extracted the phonon contribution from molecular dynamics (MD)<sup>44</sup> and the electronic contribution from experiments. Experimentally,  $\kappa(1000 \text{ K}) \approx 19 - 23$  W/mK. In UC, we obtained  $\kappa_{\text{total}} = 18.7$  W/mK, also close to the experimental value of 23 W/mK.<sup>45</sup> The discrepancy between theory and experiment is likely due to other excitations that can conduct heat but are not accounted for in our calculation, as well as the approximate nature of the Wiedemann-Franz law and Boltzmann transport theory, which are used to obtain the electronic and lattice thermal conductivity, respectively.

At last, the understanding gained from our computational study suggests avenues for improving the thermal conductivity of UC and UN. At high temperatures under which reactors operate, optimizing thermal conductivity is equivalent to minimizing resistivity. We investigate the doping dependence of the resistivity of the solid solution  $\text{UC}_{1-x}\text{N}_x$ . Here we explain how  $\text{UC}_{1-x}\text{N}_x$  solid solution can have smaller resistivity than the stoichiometric compounds, by using a set of simple interpolative equations to simulate the transport in the solid solution. The total resistivity of the is  $\rho_{\text{total}}(T) = \rho_{ee}(T) + \rho_{\text{EPI}}(T)$ , where the electron-electron interaction part can be qualitatively evaluated as  $\rho_{ee}(T) = K \frac{T^2}{T_K}$ , in which  $K$  is a constant, and  $T_K$  is the Kondo temperature  $T_K = e^{-1/N(0)J_K}$ . For the EPI part of resistivity, in order to take into account the correlation effect on the electron-phonon coupling constant, we use assume  $\lambda_{\text{eff}} = \lambda_{\text{LDA}}Z$ , where  $Z$  is the renormalization factor, which is approximately  $Z = T_K/W$ , and  $W$  is the bandwidth (here we use  $W = 2$  eV, roughly the LDA bandwidth of  $5/2$  subband of  $5f$  electrons). Since  $Z$  decreases from UC to UN as a result of of stronger electronic correlation, we assume that it changes linearly as  $Z(x) = D - Ex$  (where  $D$

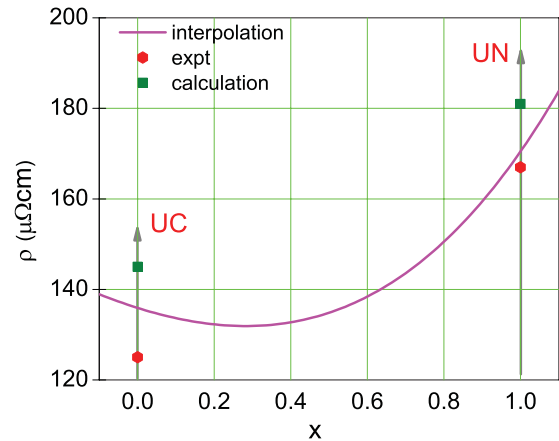


FIG. 7. (Color online) The total resistivity of  $\text{UC}_{1-x}\text{N}_x$  (solid line). The experimental and first-principles calculation results are shown at the two end points, and the interpolated curve is allowed to go between them to minimize error and give more realistic fitting.

and  $E$  are constants). From the linear-response calculations, we get  $\lambda_{\text{LDA}} = 1.3$  for UC, and 0.08 for UN. To model  $\lambda_{\text{LDA}}$  in  $\text{UC}_{1-x}\text{N}_x$  solid solution, we take the parabolic form of  $\lambda_{\text{LDA}}(x) = A - Bx + Cx^2$  (where  $A$ ,  $B$ , and  $C$  are constant fitting parameters) between the two stoichiometric UC and UN ends. At high temperatures,  $\rho_{\text{EPI}}(T)$  is a linear function of temperature, so we use  $\rho_{\text{EPI}}(T) = L\lambda_{\text{eff}}T$  (where  $L$  is a constant). Putting things together, we arrive at

$$\rho_{\text{total}}(T) = T \left( \frac{KT}{D - Ex} + L(A - Bx + Cx^2)(D - Ex) \right). \quad (4)$$

Using the quantities obtained from our LDA+DMFT and linear-response calculations for the two end points of the solution (UC and UN), we can fix the fitting parameters and plot the interpolated  $\rho_{\text{total}}(T)$  as a function of  $x$ . In Fig. 7, it is clearly seen that a minimum exists. It is also possible to achieve similar effects in UC by electron doping, or in UN by hole doping.

## V. CONCLUSION

To conclude, we have carried out an LDA+DMFT exploration of the electronic structure and transport properties of binary actinide compounds. The dioxides are charge-transfer insulators, where the Zhang-Rice state is present in  $\text{UO}_2$ . The metallic carbide and nitride compounds exhibit strong electronic correlations, which is reflected in the incoherent non-Fermi-liquid behavior at temperatures relevant for nuclear reactions. We have achieved a successful theoretical description of the transport in UC and UN, two of the most promising fuel materials due to their excellent thermophysical properties. While UN clearly shows a strongly correlated signature, both the electron-electron and electron-phonon scattering mechanisms contribute to transport in the less correlated sister compound UC. Our findings enable us to give predictions on how to improve these two uranium based nuclear fuel materials. Also, we have developed a method in

the linear-response calculation of electron-phonon interactions to include strong electron correlation effects.

#### ACKNOWLEDGMENTS

This work was supported by the United States Department of Energy Nuclear Energy University Program, Contract

No. 00088708. W.E.P. acknowledges DOE Grant No. DE-FG02-04ER46111. We acknowledge the support of Computational Materials Science Network, Grants No. DE-FG03-01ER45876, and No. DE-SC0005468 linking UC Davis and Rutgers. Q.Y. thanks Viktor Oudovenko at Rutgers University for technical support on computation.

\*leoquan@gmail.com

- <sup>1</sup>D. Butler, *Nature (London)* **429**, 238 (2004).
- <sup>2</sup>G. Kotliar, S. Y. Savrasov, K. Haule, V. S. Oudovenko, O. Parcollet, and C. A. Marianetti, *Rev. Mod. Phys.* **78**, 856 (2006).
- <sup>3</sup>X. Dai, S. Y. Savrasov, G. Kotliar, A. Migliori, H. Ledbetter, and E. Abrahams, *Science* **300**, 953 (2003).
- <sup>4</sup>J. H. Shim, K. Haule, and G. Kotliar, *Nature (London)* **446**, 513 (2007).
- <sup>5</sup>Q. Yin and S. Y. Savrasov, *Phys. Rev. Lett.* **100**, 225504 (2008).
- <sup>6</sup>K. Haule, C.-H. Yee, and K. Kim, *Phys. Rev. B* **81**, 195107 (2010).
- <sup>7</sup>P. K. Blaha, K. Schwarz, G. Madsen, D. Kvasnicka, and J. Luitz, WIEN2K package, [<http://www.wien2k.at>].
- <sup>8</sup>K. Haule, *Phys. Rev. B* **75**, 155113 (2007).
- <sup>9</sup>P. Werner, A. Comanac, L. deMedici, M. Troyer, and A. J. Millis, *Phys. Rev. Lett.* **97**, 076405 (2006).
- <sup>10</sup>[<http://www.physics.ucdavis.edu/mindlab>].
- <sup>11</sup>S. Y. Savrasov, *Phys. Rev. Lett.* **69**, 2819 (1992).
- <sup>12</sup>S. Y. Savrasov and D. Y. Savrasov, *Phys. Rev. B* **54**, 16487 (1996).
- <sup>13</sup>A. Kutepov, K. Haule, S. Y. Savrasov, and G. Kotliar, *Phys. Rev. B* **82**, 045105 (2010).
- <sup>14</sup>T. Ejima, K. Murata, S. Suzuki, T. Takahashi, S. Sato, T. Kasuya, Y. Ōnuki, H. Yamagami, A. Hasegawa, and T. Ishii, *Physica B* **186–188**, 77 (1993).
- <sup>15</sup>M. Samsel-Czekala, E. Talik, P. de V. Du Plessis, R. Troc, H. Misiorek, and C. Sułkowski, *Phys. Rev. B* **76**, 144426 (2007).
- <sup>16</sup>L. Havela, F. Wastin, J. Rebizant, and T. Gouder, *Phys. Rev. B* **68**, 085101 (2003).
- <sup>17</sup>T. Gouder, P. M. Oppeneer, F. Huber, F. Wastin, and J. Rebizant, *Phys. Rev. B* **72**, 115122 (2005).
- <sup>18</sup>T. Ito, H. Kumigashira, T. Takahashi, E. Yamamoto, Y. Haga, and Y. Onuki, *J. Magn. Magn. Mater.* **226–230**, 40 (2001).
- <sup>19</sup>M. Yoshizawa and T. Suzuki, *J. Magn. Magn. Mater.* **90–91**, 523 (1990).
- <sup>20</sup>Ionut D. Prodan, Gustavo E. Scuseria, and Richard L. Martin, *Phys. Rev. B* **73**, 045104 (2006).
- <sup>21</sup>Ionut D. Prodan, Gustavo E. Scuseria, and Richard L. Martin, *Phys. Rev. B* **76**, 033101 (2007).
- <sup>22</sup>H. Y. Geng, Y. Chen, Y. Kaneta, and M. Kinoshita, *Phys. Rev. B* **75**, 054111 (2007).
- <sup>23</sup>Bao-Tian Wang, Hongliang Shi, Weidong Li, and Ping Zhang, *Phys. Rev. B* **81**, 045119 (2010).
- <sup>24</sup>Bo Sun, Ping Zhang, and Xian-Geng Zhao, *J. Chem. Phys.* **128**, 084705 (2008).
- <sup>25</sup>Y. Baer and J. Schoenes, *Solid State Commun.* **33**, 885 (1980).
- <sup>26</sup>M. T. Butterfield, T. Durakiewicz, E. Guziewicz, J. J. Joyce, A. J. Arko, K. S. Graham, D. P. Moore, and L. A. Morales, *Surf. Sci.* **571**, 74 (2004).
- <sup>27</sup>J. Zaanen, G. A. Sawatzky, and J. W. Allen, *Phys. Rev. Lett.* **55**, 418 (1985).
- <sup>28</sup>Q. Yin, A. Gordienko, X. Wan, and S. Y. Savrasov, *Phys. Rev. Lett.* **100**, 066406 (2008).
- <sup>29</sup>F. C. Zhang and T. M. Rice, *Phys. Rev. B* **37**, 3759 (1988).
- <sup>30</sup>O. Gunnarsson and O. Rösch, *J. Phys.: Condens. Matter* **20**, 043201 (2008).
- <sup>31</sup>W. J. L. Buyers, A. F. Murray, T. M. Holden, E. C. Svensson, P. de V. Du Plessis, G. H. Lander, and O. Vogt, *Physica B* **102**, 291 (1980).
- <sup>32</sup>K. P. Bohnen, R. Heid, and M. Krauss, *Europhys. Lett.* **64**, 104 (2003).
- <sup>33</sup>L. Boeri, O. V. Dolgov, and A. A. Golubov, *Phys. Rev. Lett.* **101**, 026403 (2008).
- <sup>34</sup>S. Y. Savrasov, K. Haule, and G. Kotliar, *Phys. Rev. Lett.* **96**, 036404 (2006).
- <sup>35</sup>S. Y. Savrasov and G. Kotliar, *Phys. Rev. Lett.* **90**, 056401 (2003).
- <sup>36</sup>G. D. Gaspari and B. L. Gyorffy, *Phys. Rev. Lett.* **28**, 801 (1972).
- <sup>37</sup>D. A. Papaconstantopoulos, L. L. Boyer, B. M. Klein, A. R. Williams, V. L. Moruzzi, and J. F. Janak, *Phys. Rev. B* **15**, 4221 (1977).
- <sup>38</sup>I. I. Mazin, E. M. Savitski, and Y. A. Uspenski, *Phys. Status Solidi B* **112**, 29 (1982).
- <sup>39</sup>H. Matsui, M. Tamaki, S. Nasu, and T. Kurasawa, *J. Phys. Chem. Solids* **41**, 351 (1980).
- <sup>40</sup>P. Costa and R. Lallement, *Phys. Lett.* **7**, 21 (1973).
- <sup>41</sup>S. Carniglia, *Carbides in Nuclear Energy*, edited by L. Russell *et al.* (Macmillan, London, 1964), Vol. 1, p. 365.
- <sup>42</sup>W. Fulkerson, T. G. Kollie, S. C. Weaver, J. P. Moore, and R. K. Williams, *Pu 1970 and Other Actinides*, edited by W. Miner (Jack V. Richard, Executive Publisher, New York, 1970), Part 2, p. 374.
- <sup>43</sup>T. Ohmichi, T. Kikuchi, and S. J. Nasu, *Nucl. Sci. Technol.* **9**, 77 (1972).
- <sup>44</sup>K. Kurosaki, K. Yano, K. Yamada, M. Uno, and S. A. Yamanaka, *J. Alloys Compd.* **311**, 305 (2000).
- <sup>45</sup>R. De Coninck, W. Van Lierde and A. Gijs, *J. Nucl. Mater.* **57**, 69 (1975).